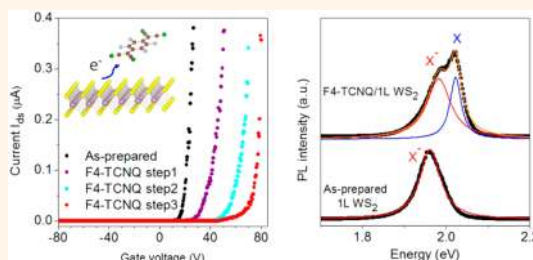


Chemically Driven Tunable Light Emission of Charged and Neutral Excitons in Monolayer WS₂

Namphung Peimyoo,[†] Weihuang Yang,[†] Jingzhi Shang,[†] Xiaonan Shen,[†] Yanlong Wang,[†] and Ting Yu^{*†,‡,§}

[†]Division of Physics and Applied Physics, School of Physical and Mathematical Sciences, Nanyang Technological University, Singapore 637371, [‡]Department of Physics, Faculty of Science, National University of Singapore, Singapore 117542, and [§]Graphene Research Centre, National University of Singapore, 2 Science Drive 3, Singapore 117542

ABSTRACT Monolayer (1L) semiconducting transition metal dichalcogenides (TMDs) possess remarkable physical and optical properties, promising for a wide range of applications from nanoelectronics to optoelectronics such as light-emitting and sensing devices. Here we report how the molecular adsorption can modulate the light emission and electrical properties of 1L WS₂. The dependences of trion and exciton emission on chemical doping are investigated in 1L WS₂ by microphotoluminescence (μ PL) measurements, where different responses are observed and simulated theoretically. The total PL is strongly enhanced when electron-withdrawing molecules adsorb on 1L WS₂, which is attributed to the increase of the exciton formation due to charge transfer. The electrical transport measurements of a 1L WS₂ field effect transistor elucidate the effect of the adsorbates on the conductivity, which give evidence for charge transfer between molecules and 1L WS₂. These findings open up many opportunities to manipulate the electrical and optical properties of two-dimensional TMDs, which are particularly important for developing optoelectronic devices for chemical and biochemical sensing applications.



KEYWORDS: tungsten disulfide · photoluminescence · exciton · trion · chemical doping · charge transfer

Layer structures of transition metal dichalcogenides (TMDs) have received considerable research interest due to their striking optical and electrical properties,^{1–3} especially semiconducting WS₂, WSe₂, MoS₂, and MoSe₂ layers. Their bulk crystals are indirect band gap semiconductors, while monolayers own direct band gaps corresponding to the visible to near-infrared photon energies,¹ making them more suitable than graphene for light-emitting and functional transistor applications. Recently, those semiconducting TMDs have been explored for optoelectronics such as light-emitting diodes,^{4–7} photodetectors,⁸ and solar cells.⁴ Furthermore, unique symmetry and strong spin–orbital coupling enable these TMD layers to serve as a new platform for valleytronic research.^{9–11}

The optical response of 1L TMDs is dominated by excitonic transitions: A and B excitons as observed in the optical absorption and emission spectra,^{12–14} originating from the splitting of the valence band maximum at the K (K') point due to the large

spin–orbital interactions. The large exciton binding energies in 1L TMDs have been predicted to be 0.5–1 eV.^{15–17} In 1L WS₂, a binding energy as high as 0.5–0.7 eV has recently been extracted by temperature-dependent photoluminescence and two-photon absorption measurements.^{14,18} It is also known that the concentrations of the negatively (X[−]) or positively (X⁺) charged excitons (so-called trions) and neutral excitons (X) in semiconducting quantum wells and quantum dots can be modulated by applying gate voltage,¹⁹ chemical doping,²⁰ or laser excitation.^{21–23} Recently, electrical doping measurements of 1L MoSe₂²⁴ and WSe₂²⁵ have shown the tunability of the excitonic species among X[−], X, and X⁺, and electrically tunable emission between X[−] and X components has been observed in MoS₂ and WS₂.^{18,26} It is also worth noting that chemical doping *via* the absorption of gases and organic molecules has become a promising approach to tune charge carriers in graphene^{27,28} and some TMDs.^{29,30} By contrast, controlling the excitonic species

* Address correspondence to yuting@ntu.edu.sg.

Received for review July 29, 2014 and accepted October 15, 2014.

Published online October 15, 2014
10.1021/nn504196n

© 2014 American Chemical Society

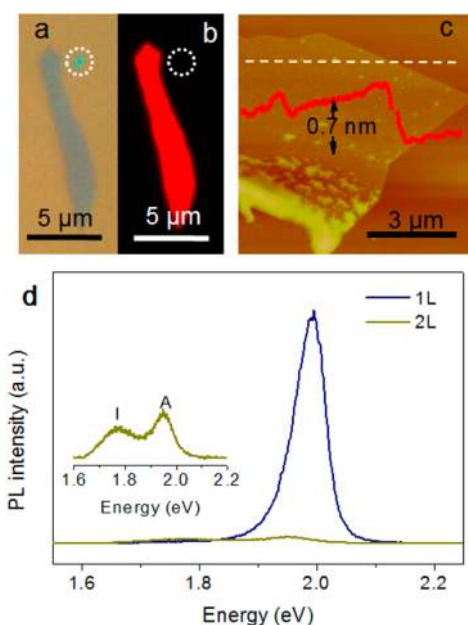


Figure 1. Characterization of WS₂ flakes. Optical microscope image of WS₂ flakes (a) and the corresponding fluorescence image (b), where the thick WS₂ flake is circled. (c) Atomic force microscope (AFM) image of a WS₂ flake. Inset is the AFM height profile along the dashed line. (d) Photoluminescence (PL) spectra of 1L and bilayer (2L) WS₂ excited by a 532 nm laser. Inset: Enlarged spectrum of a 2L presenting an indirect band gap labeled as I.

in semiconducting 1L WS₂ *via* chemical doping is still less explored now. Particularly, H₂O molecules commonly exist in fabrication processes and operation environments of most semiconductor devices. In view of the very promising prospects of 1L WS₂ for light-emitting device applications, studying the influence of H₂O on the light emission is very meaningful, while it has not received enough attention until now.

In this work, we demonstrate the tunability of charged and neutral excitons in 1L WS₂ *via* chemical doping (F₄TCNQ and H₂O molecules) as characterized by micro-photoluminescence (PL) spectroscopy. The electrical transport data suggest that the exfoliated 1L WS₂ is a naturally n-type semiconductor and clearly delineates that the electron concentration decreases when the electron-withdrawing dopant interacts with WS₂. Moreover, it is found that adsorption of electron-withdrawing molecules strongly enhances the total PL by charge transfer. The changes of neutral and charged excitons are well modeled by a simplified theoretical framework. Our work demonstrates the ability of chemical doping to tune the excitonic emission species in 1L WS₂ and clarifies the charge transfer mechanism, which is very important for exploiting the TMDs for optoelectronic and chemical sensing applications.

RESULTS AND DISCUSSION

WS₂ flakes were mechanically exfoliated from the commercial WS₂ crystals onto the 300 nm thick SiO₂ on a highly doped Si wafer. Figure 1a and b show the

optical micrograph of WS₂ flakes and the corresponding fluorescence image, respectively, in which striking emission is observed in the 1L region, while there is no detectable emission signal from the thicker counterpart. Hence, the fluorescence image can be used to rapidly distinguish a single layer from multilayers. The thicknesses of WS₂ flakes are further characterized by atomic force microscopy (AFM) and photoluminescence measurements. In Figure 1c, the AFM image shows the topological surface of a representative WS₂ sample, and its line scan along the white dashed line in the 1L region presents an average height of 0.7 nm.

Figure 1d shows room-temperature PL spectra of 1L and 2L WS₂ characterized by PL spectroscopy using 2.33 eV laser excitation, where the pronounced peak at around 1.98 eV is observed and it may contain the emission from both neutral and charged A exciton states. Note that the B exciton feature is not measurable under this laser excitation. The energy difference between the A and B excitons arises from the splitting of the valence band due to spin–orbital coupling, which is found to be ~0.4 eV for 1L and multilayer WS₂.^{17,31} The PL of 1L WS₂ is much more intense than that of 2L, which is strong evidence of the direct to indirect transition. The inset clarifies the spectral features for 2L, where the indirect band gap transition is denoted as I. The direct transition in 1L WS₂ occurs between the valence band maximum and conduction band minimum, located at the K point of the Brillouin zone according to theoretical predictions^{16,32} and photoemission experiment.³³ In multilayer and bulk WS₂, indirect radiative recombination exists, which involves the transition from either the K point or the midpoint along K and Γ of the conduction band to the Γ point of the valence band.^{32,34–36}

Adsorbates and the surrounding environment can greatly tailor the electrical and optical properties of 2D semiconductors. Particularly, the effective modification of carrier concentrations in such atomically thin semiconductors may lead to very promising electronic and optoelectronic device applications. Here, a strong electron-withdrawing molecule of 2,3,5,6-tetrafluoro-7,7,8,8-tetracyanoquinodimethane (F₄TCNQ) has been utilized to modulate the properties of 1L-WS₂. To examine the effect of the molecular adsorption on the electrical properties of 1L WS₂, a back-gated field effect transistor (FET) was fabricated. Meanwhile, the step doping technique³⁰ has been used to deposit the molecules on 1L WS₂, and the electrical transport data were recorded under various doping steps. One doping step mainly includes two processes: one is the drop casting of the molecular solution on the targeted sample; the other is drying in ambient condition (see Methods). This technique is effective to tune the carrier concentration in 1L WS₂ as demonstrated in the following transport data. The 1L WS₂ device configuration is schematically shown in Figure 2a. Figure 2b is an

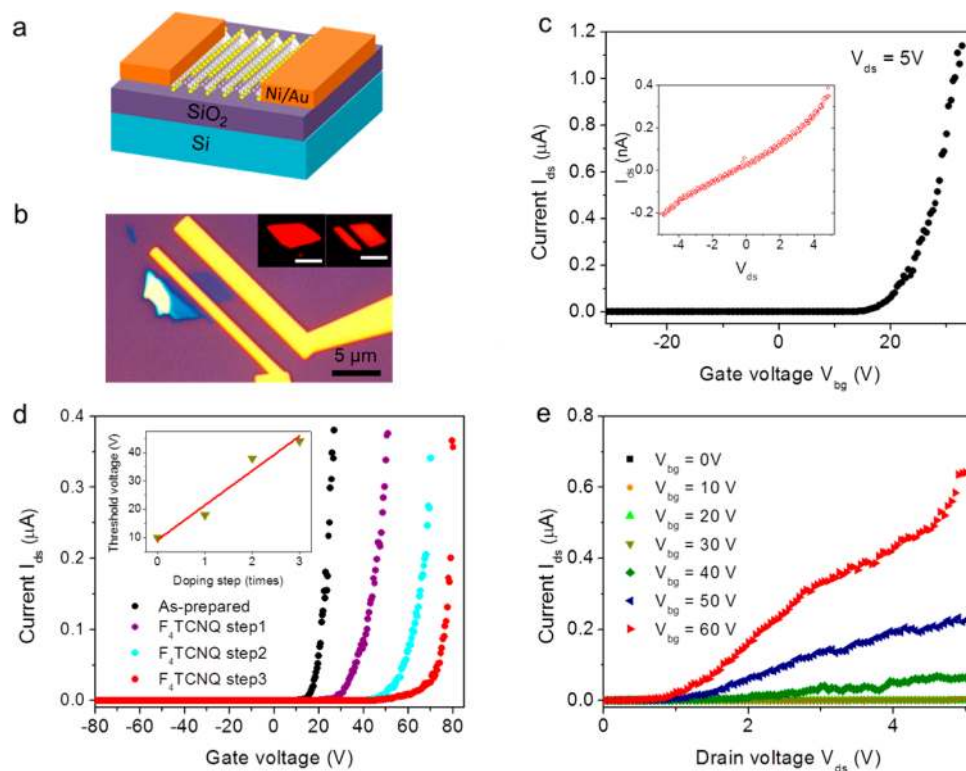


Figure 2. Electrical transport characteristics of 1L WS₂ and F₄TCNQ/1L WS₂ at room temperature in a vacuum. (a) Schematic of the back-gated field effect transistor (FET) of 1L WS₂. (b) Optical micrograph of a 1L WS₂ device. Inset shows fluorescence images of WS₂ before (left) and after (right) device fabrication, respectively. (c) Transport characteristic of the WS₂ FET before the F₄TCNQ modification when $V_{ds} = 5$ V. Inset: Drain current versus bias voltage ($I_{ds}-V_{ds}$) curve acquired at $V_{bg} = 0$ V. (d) $I_{ds}-V_{bg}$ curves under $V_{ds} = 5$ V of the as-prepared sample and after various F₄TCNQ doping steps. Inset: Threshold voltage as a function of doping step. (e) $I_{ds}-V_{ds}$ curves of F₄TCNQ/1L WS₂ after doping step 3 recorded for different V_{bg} values.

optical image of the 1L WS₂ FET device, fabricated by standard electron-beam lithography. Insets of Figure 2b are fluorescence images of 1L WS₂ before and after device fabrication, which indicate that the intense emission can be preserved after the FET fabrication. The electrical transport characteristic of as-exfoliated 1L WS₂ has been measured at the bias voltage V_{ds} of 5 V under vacuum conditions, which shows the n-type behavior (Figure 2c). The native n-type doping in 1L WS₂ is similar to 1L MoS₂,^{26,37} which probably arises from the structural defects and/or substrate effects. At the bias voltage $V_{ds} = 5$ V, the on-off current ratio of our device is approximately 10^5 . The inset of Figure 2c is the typical output ($I_{ds}-V_{ds}$) characteristic of the as-exfoliated WS₂ FET acquired at $V_{bg} = 0$ V. We can estimate the carrier mobility from Figure 2c using the equation $\mu = [dI_{ds}/dV_{bg}] \times [L/WC_gV_{ds}]$, where L and W are channel length (6.5 μm) and width (4 μm), respectively, and C_g is the gate capacitance per unit area (1.15×10^{-4} F m⁻² for a 300 nm thick SiO₂ layer). The electron mobility is calculated to be $9.5 \text{ cm}^2 \text{ V}^{-1} \text{ s}^{-1}$, which is larger than some reported values for CVD-grown 1L WS₂,^{38,39} comparable to those obtained from the exfoliated 1L MoS₂ with similar device structures,^{40,41} and smaller than that of the exfoliated 1L WS₂ device using the ionic liquid gate ($44 \text{ cm}^2 \text{ V}^{-1} \text{ s}^{-1}$).⁵

Figure 2d shows representative electrical transport curves of 1L WS₂ before and after F₄TCNQ doping at various steps. After depositing F₄TCNQ for the first time, the threshold voltage shifts to the positive region by 10 V with respect to that of the as-prepared device. As the doping step increases, it significantly shifts further toward positive voltages, which suggests the effective reduction of the electron concentration in the conduction band. The threshold voltage as a function of doping step is plotted as shown in the inset of Figure 2d. Note that the effects of moisture adsorption may also cause the shift of the threshold voltage,⁴⁰ but it can be negligible here, as the measurements were conducted in the vacuum condition ($\sim 10^{-5}$ mbar). The transport data elucidate that the electrons transfer from n-type 1L WS₂ to F₄TCNQ molecules, corresponding to a neutralization process of 1L WS₂. Figure 2e shows the $I_{ds}-V_{ds}$ characteristics of 1L WS₂ after the third round of doping at various gate voltages. The shape of the $I_{ds}-V_{ds}$ curve indicates the occurrence of Schottky barrier contacts in the 1L WS₂ FET, consistent with the recent study of a 1L MoS₂ device using Ti/Au contacts.⁴² More importantly, by adjusting the back-gate voltage, the conductivity of the F₄TCNQ/1L WS₂ can be modulated in a controllable manner.

After studying the chemical doping effect on the electrical transport properties, we further investigated

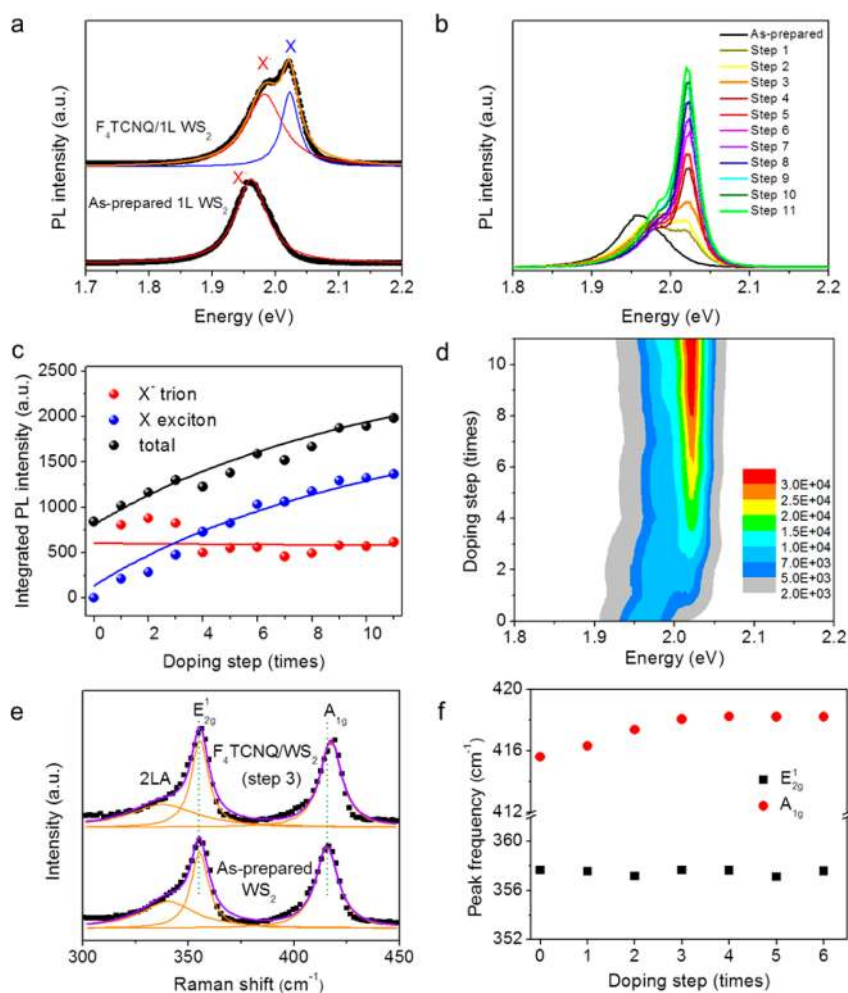


Figure 3. Tunable photoluminescence and Raman scattering driven by molecular adsorbates. (a) Room-temperature PL spectra of 1L WS₂ before and after doping with F₄TCNQ. (b) PL spectra upon consecutive F₄TCNQ doping. (c) Integrated PL intensities of X⁻, X, and the sum as a function of doping step. Solid lines are the theoretical calculation results based on the rate equation. (d) PL intensity map (in counts) as a function of doping step and photon energy. (e) Raman spectra of the 1L WS₂ and F₄TCNQ/1L WS₂ under 457 nm laser excitation. (f) Peak frequencies of the E¹₂₀ and A₁₀ modes versus doping step.

the influence of molecular adsorption on the optical properties of 1L WS₂. Figure 3a shows that the main emission of the as-exfoliated 1L WS₂ is observed at around 1.96 eV, which may be the emission from neutral and/or charged A exciton states according to previous studies.^{18,26} After the adsorption of F₄TCNQ molecules, the PL features clearly evolve into two distinct components, which can be well fitted by two Lorentzian peaks located at around 1.98 and 2.02 eV, respectively. Note that the higher energy emission in the F₄TCNQ/1L WS₂ sample is fully absent in the PL spectrum of the as-exfoliated sample, while the lower energy peak in the F₄TCNQ/1L WS₂ shows a very similar profile to the emission peak of the 1L WS₂. Our findings of the transport measurements discussed above indicate that 1L WS₂ is an n-type semiconductor. Hence, the emission peak observed in the as-prepared 1L WS₂ sample is mainly attributed to the negatively charged trion (X⁻) emission, i.e., an electron-bound exciton, whereas the higher energy peak emerging after F₄TCNQ adsorption is assigned to the neutral exciton

(X). In other words, the suppression of the exciton emission in the as-prepared 1L WS₂ is due to the unintentional n-type doping. In 1L WS₂, one previous study shows that the trion emission can be observed only at low temperatures under high excitation laser powers,⁴³ while a very recent report illustrates that both the trion and exciton emission can be observed at room temperature.¹⁸ The PL discrimination from these 1L WS₂ samples is attributed to the different electron densities from sample to sample, as demonstrated in the following. The evolution of PL spectra under successive doping (Figure 3b) shows that the X⁻ and X emission changes differently with doping. As the doping step increases, the PL intensity of the X is remarkably enhanced, while the X⁻ is nearly unchanged. Figure 3c shows the integrated intensity of each component and the total intensity as a function of doping step, where the details of the spectral fitting are included in the Supporting Information (see Figure S1). In the as-prepared 1L WS₂, the spectral weight of the X⁻ peak is predominant because it is rich in free

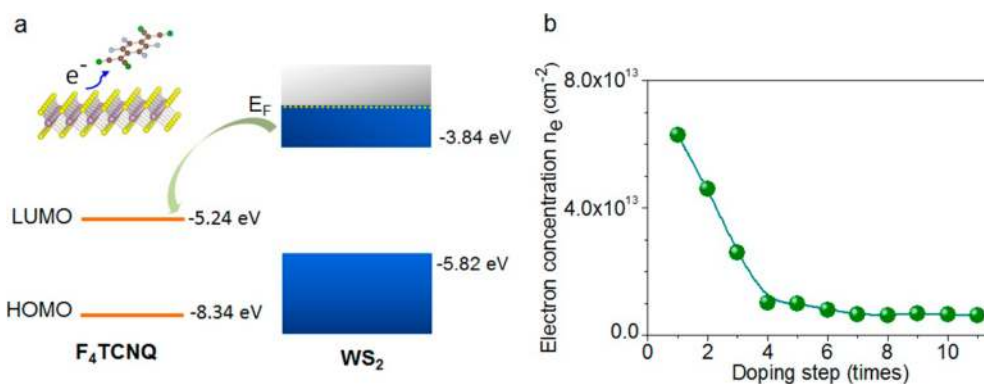


Figure 4. (a) Schematic of charge transfer between 1L WS₂ and F₄TCNQ. (b) Calculated electron concentration as a function of F₄TCNQ doping step.

electrons, leading to the increase of the probability of X⁻ formation. Upon consecutive doping induced by the F₄TCNQ adsorption, the integrated PL intensity of the X is monotonically enhanced, whereas the integrated intensity of X⁻ displays a slight reduction. Above the doping step 9, the PL intensity of the X has the tendency to saturate. The electrical gating effect on PL in 1L WS₂ has been measured,¹⁸ which supports our arguments. Theoretically, the dependences of the total intensity and the intensities of X and X⁻ on doping have been calculated according to a rate equation and a mass-action law,^{23,24,30,44} as denoted by the solid curves (Figure 3c), which agree fairly well with the experimental data. The details of our theoretical model are presented later.

Figure 3d shows the PL intensity map as a function of photon energy and doping step. The peak position of X⁻ blue-shifts with the increase in F₄TCNQ adsorption, while that of X remains almost unchanged with doping. The fit results are shown in Figure S2. The typical trion dissociation energy determined from the energy difference between the X and X⁻ is found to be ~38 meV, in agreement with those obtained from the electrical gated 1L WS₂ device.¹⁸ The trion dissociation energy decreases with the increase in deposited molecules or the decreased electron doping in 1L WS₂, as shown in Figure S2, similar to the observation in electrically controlled PL for 1L MoS₂ and WSe₂.^{25,26} The observed trion dissociation energy is much larger than those of typical semiconductor quantum wells and quantum dots (typically in the range 1–6 meV),^{19,20,23,45} which indicates the larger excitonic effect in such a 2D semiconductor.

Besides the doping effect discussed above, strain can also affect the PL intensity and the band gap of ultrathin TMD materials. For instance, when strain is applied in 1L MoS₂, the near-band-edge emission changes.^{46,47} Raman measurements were conducted before and after doping, in order to exclude the effect of strain on the PL change in our case. Figure 3e shows Raman spectra of the as-exfoliated 1L WS₂ and the F₄TCNQ/1L WS₂. The variations of their peak

frequencies with doping are presented in Figure 3f. It is found that the A_{1g} mode slightly blue-shifts by 2 cm⁻¹ after the early few steps of F₄TCNQ deposition, while the peak position of the E¹_{2g} mode does not change. As known, in a typical 1L TMD, the out-of-plane A_{1g} mode is susceptible to the charging effect and red-shifts with the electron doping, but the in-plane E¹_{2g} mode is not affected by the doping effect, which is due to the strong electron–phonon coupling with the out-of-plane mode.⁴⁸ On the contrary the E¹_{2g} mode has been shown to be sensitive to strain and red-shifted with increasing of both uniaxial and biaxial strain, while the A_{1g} mode remains unchanged.^{47,49} Thus, our observed Raman features indicate the F₄TCNQ/1L WS₂ sample is less n-doped than that of 1L WS₂ due to the charge transfer during F₄TCNQ adsorption; the strain effect in the F₄TCNQ/1L WS₂ sample is negligible. These Raman studies agree well with both electrical transport and PL data above.

The PL modulation of X⁻ and X in WS₂ due to F₄TCNQ adsorption can be understood in terms of charge transfer, which results from the band alignments of WS₂ and the dopant. Figure 4a shows the calculated minimum conduction band (-3.84 eV) and maximum valence band (-5.82 eV) of WS₂⁵⁰ and the F₄TCNQ HOMO (-8.34 eV) and LUMO (-5.24 eV).⁵¹ Since 1L WS₂ is natively n-type here, the free electrons occupy the bottom of the conduction band. Due to the band offset between 1L WS₂ and F₄TCNQ, the electrons transfer from 1L WS₂ to F₄TCNQ, resulting in the neutralization of 1L WS₂ and the reduction of the probability of trion formation. The more F₄TCNQ adsorption, the more electrons withdraw from the naturally n-type 1L WS₂. Therefore, an enhancement in the exciton intensity in 1L WS₂ modified with F₄TCNQ molecules is observed, while the trion spectral weight diminishes. Furthermore, we have simulated the charge transfer when a F₄TCNQ molecule sits on a defined WS₂ unit cell. As shown in Table S1, the F₄TCNQ molecule withdraws a charge of 0.1e from 1L WS₂, which supports the argument above.

Our measurements indicate that the PL intensity of 1L WS₂ is sensitive to the adsorption of dopant molecules. In theory, the responses of the PL intensities from trion and exciton states in 1L WS₂ under F₄TCNQ doping can be modeled by a rate equation and a mass-action law.^{23,24,30,44} The three-level model is used as shown in the schematic (Figure S3) presenting photoexcitation (*G*), the neutral exciton recombination (*X*), the trion recombination (*X*⁻), and the trion formation (*F*_{tr}). The trion formation $F_{tr} = k_{tr}(n)N_x$, where N_x is the population of excitons, $k_{tr}(n)$ is the trion formation rate, and n is the doping step.³⁰ By solving the rate equation under steady-state conditions, the dependences of I_x , I_{X^-} , and the total intensity on doping were calculated (see Supporting Information) and are shown by the blue, red, and black solid lines, respectively (Figure 3c). Our calculated results agree well with the experimental data.

The relationship among the concentrations of trions (N_{X^-}) and excitons (N_x) and the charge carrier density (n_e) in semiconductors was proposed based on the law of mass action,^{23,24,44} written as

$$\frac{N_x n_e}{N_{X^-}} = \left(\frac{4m_x m_e}{\pi \hbar^2 m_{X^-}} \right) k_B T \exp\left(-\frac{E_b}{k_B T} \right) \quad (1)$$

where \hbar is the reduced Planck's constant, k_B is the Boltzmann constant, T is the temperature, E_b is the trion binding energy, m_e is effective mass of electrons, and m_{X^-} and m_x are trion and exciton effective masses, respectively, where $m_{X^-} = 2m_e + m_h$ and $m_x = m_e + m_h$. According to the theoretical calculation,¹⁷ m_e and m_h are $0.44m_0$ and $0.45m_0$, respectively, where m_0 is the mass of a free electron.

The concentrations of trions and excitons are proportional to their PL intensities, and therefore the integrated intensity ratio of I_{X^-} to I_x can be written as³⁰

$$\frac{I_{X^-}}{I_x} = \frac{\gamma_{tr}}{\gamma_{ex}} \left(\frac{\pi \hbar^2 m_{X^-}}{4m_x m_e} \right) \frac{n_e}{k_B T} \exp\left(\frac{E_b}{k_B T} \right) \quad (2)$$

where γ_{tr} and γ_{ex} are radiative decay rates of trions and excitons obtained from fitting parameters in rate equations, respectively. By fitting the I_{X^-}/I_x ratio in eq 2, the electron concentration in 1L WS₂ as a function of doping step is calculated as shown in Figure 4b. The initial electron concentration of the as-exfoliated 1L WS₂ can be extrapolated based on the nearly linear range in the first four doping steps, and the estimated value is $\sim 8 \times 10^{13} \text{ cm}^{-2}$. The electron concentration drastically drops to $\sim 1 \times 10^{13} \text{ cm}^{-2}$ after the F₄TCNQ doping step 4. After that it gradually decreases and finally reaches saturation ($\sim 6 \times 10^{12} \text{ cm}^{-2}$). Our results emphasize that the physical adsorption of dopants can tune the carrier concentration in 1L WS₂ and strongly modulate its optical and electrical properties, which are expected to be a generic effect for other layered TMD materials as well. In particular, the sensitivity of

the excitonic species of 1L WS₂ to the molecular absorption can be used for optoelectronic and chemical sensing applications. Note that the as-exfoliated 1L WS₂ here is highly n-doped, as reflected in the suppression of the exciton peak. Similarly, the highly n-doped behavior has also been observed ($\sim 6 \times 10^{13} \text{ cm}^{-2}$) in exfoliated 1L MoS₂.³⁰ Such unintentional doping is probably related to the substrate condition^{52–54} and the crystal quality.^{14,55} In detail, one possibility is that the doping comes from trap states at the interface between WS₂ and the substrate. Scheuschener *et al.* have reported the n-type doping of 1L MoS₂ is induced by the substrate, where the trion X^- or the exciton X peak is dominant in the supported or free-standing sample, respectively.⁵³ Theoretical calculations show that the conductivity of 1L MoS₂ can be modulated from n- to p-type when MoS₂ is placed onto a SiO₂ substrate with the presence of different defects and impurities at the interface.⁵⁴ Another argument on the origin of n-type conductivity is intrinsic structural defects such as monosulfur vacancy (V_S) and disulfur vacancy (V_{S_2}). Intrinsic defects have been directly observed by scanning transmission electron microscopy in monolayer MoS₂ and WS₂.^{55,56} According to first-principles calculations based on density functional theory, some of these defects can introduce additional donor and/or acceptor levels and cause effective doping in such 1L semiconductors.⁵⁵

Moreover, it has been noted that gas and H₂O absorption can affect the optical and electrical properties of MoS₂.^{29,40,57} In particular, H₂O is extensively used in most practical fabrication processes of electronic and optoelectronic devices and often exists in their operation atmospheres. Therefore, knowledge on the effect of H₂O on PL of 1L WS₂ is very important, which is explored here. In our experiments, H₂O was simply drop-casted onto the WS₂ surface, which was then covered by a glass coverslip. The PL spectra were recorded at various times to monitor their change induced by the interactions between H₂O and 1L WS₂. Figure 5a depicts the PL spectra of the as-prepared 1L WS₂ and the H₂O-covered 1L WS₂ for 5 and 50 min, respectively. Three spectra are fitted by two Lorentzian components denoted as X^- and X to estimate the influence of H₂O adsorption on the evolution of the PL line shape. The detailed analysis of the integrated intensity of each component as a function of adsorption time (Figure 5b) shows that in the as-prepared sample the X^- occupies a larger spectral weight than X . With the increase in adsorption time, the integrated PL intensity of X^- mostly does not change over time, whereas the PL intensity of X is enhanced, analogous to the effect caused by F₄TCNQ as shown above. In order to further clarify the time-dependent PL behavior of H₂O/1L WS₂, we have performed charge transfer calculations of three kinds of configurations, as shown in Table 1. Note that the small binding energy is

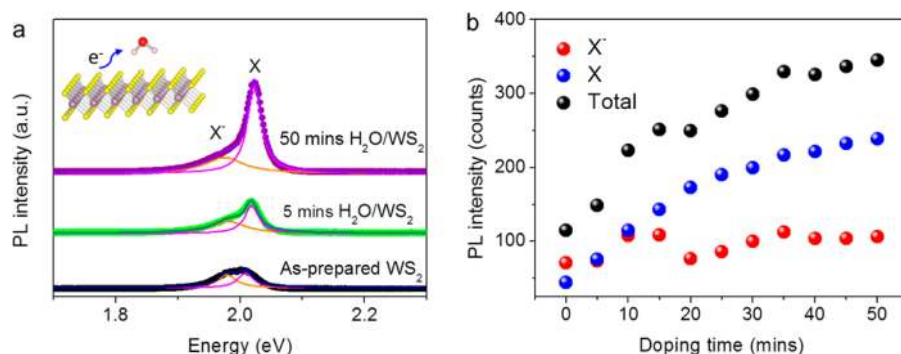


Figure 5. Effect of H₂O adsorption on PL of 1L WS₂. (a) Evolution of 1L WS₂ PL spectra upon H₂O adsorption recorded at different times. Inset shows the charge transfer. (b) Dependence of the integrated PL intensities of trion and exciton components on the doping time.

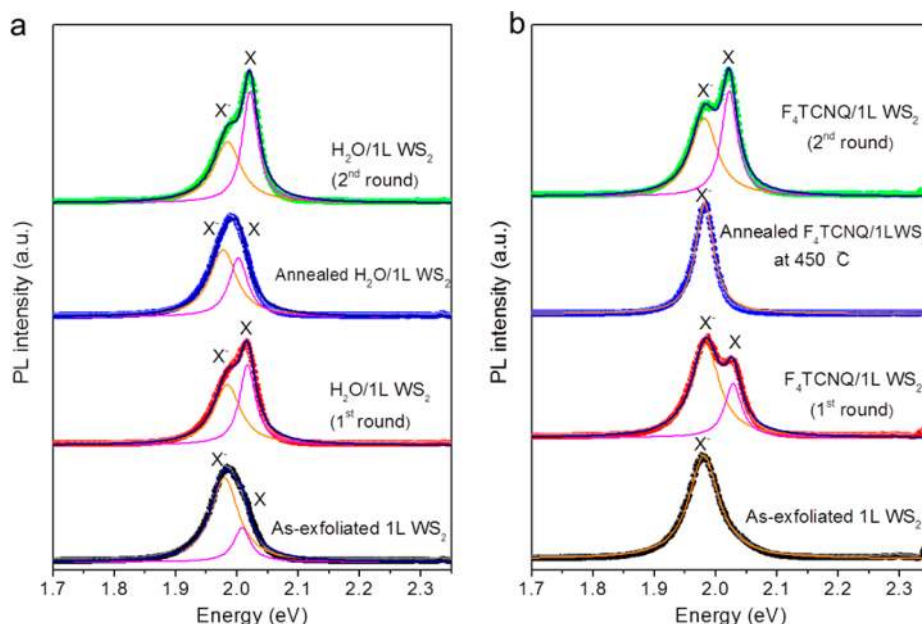


Figure 6. Annealing effects on the trion and exciton emission. (a) PL spectra of as-exfoliated WS₂, H₂O/1L WS₂, and H₂O/1L WS₂ after annealing at 150 °C in air for 20 min and redoping of the annealed sample. (b) PL spectra of as-exfoliated WS₂, F₄TCNQ/1L WS₂, and F₄TCNQ/1L WS₂ after annealing at 450 °C under vacuum for 20 min and F₄TCNQ/1L WS₂ (second round).

indicative of physical adsorption, which is in the same order as the O₂ adsorption on 1L MoS₂.⁵⁸ A charge of 0.09e transfers from the WS₂ layer to H₂O when the 4 × 4 WS₂ unit cell adsorbs a H₂O molecule. When two independent H₂O molecules are adsorbed on WS₂, two H₂O molecules withdraw 0.11e from the WS₂ cell. When more H₂O molecules adsorb on WS₂, the coupling or interaction among these molecules becomes important. For example, when two coupled H₂O molecules adsorb on WS₂, these two H₂O can obtain 0.16e from the WS₂ cell, which is more than that obtained by two independent H₂O molecules. Thus, the PL change with time is attributed to more electrons transferred from 1L WS₂ to H₂O molecules, which is caused by the increasing number of adsorbed H₂O molecules and the presence of coupling among these molecules.

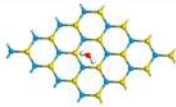
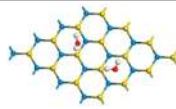
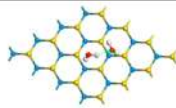
Finally, we investigate the annealing effects on the light emission from trion and exciton states of H₂O/1L WS₂ and F₄TCNQ/1L WS₂ samples (Figure 6a and b). It is

found that after annealing the emission spectral weight of excitons in both H₂O- and F₄TCNQ-attached 1L WS₂ substantially decreases (it vanishes for F₄TCNQ-doped sample), indicating the removal of the molecular dopants. As a result, these samples become more n-doped than they do without annealing, i.e., a recovery process of n-type doping in 1L WS₂. Furthermore, H₂O and F₄TCNQ molecules were redeposited on the same annealed samples for the second round. As seen in Figure 6, the X spectral weight increases and it is larger than that of X⁻. The results suggest that the evolution of the X⁻ and X features is reversible in 1L WS₂ via our chemical doping and thermal annealing, which provides more flexibility for potential device applications.

CONCLUSIONS

We have demonstrated that neutral and charged exciton emission can be tuned through adsorption of the electron-withdrawing dopants of F₄TCNQ and H₂O.

TABLE 1. Calculated Binding Energies and Charge Transfer in Different H₂O/WS₂ Configurations^a

Sample	Structure	Binding energy (eV)	Charge transfer (e ^a)
H ₂ O-WS ₂		-0.214	0.09
2H ₂ O-WS ₂		-0.362	0.11
Coupled 2H ₂ O-WS ₂		-0.329	0.16

^a The charge that molecules obtain from the WS₂ layer is analyzed by the Hirshfeld method.

The PL enhancement upon successive doping is due to the increment of exciton formation, while the formation of trions is weakened, as a consequence of the electron transfer from 1L WS₂ to the dopants. The electrical transport measurements confirm that the n-type semiconducting behavior is a characteristic of the used as-exfoliated samples and elucidate that the

adsorption of F₄TCNQ molecules reduces the electron concentration in 1L WS₂. Our studies develop a very efficient approach to control the excitonic emission species in 1L WS₂ and reveal the corresponding charge transfer mechanism, which is significant for optoelectronics and chemical sensing applications of 2D TMDs.

METHODS

Photoluminescence Spectroscopy. WS₂ flakes were produced by mechanical exfoliation from commercial WS₂ crystals (2D Semiconductors Inc.) onto the 300 nm thick SiO₂ on the highly doped Si wafer. The number of layers of WS₂ flakes was determined by atomic force microscopy, fluorescence, and photoluminescence spectrometers. Micro-PL and Raman measurements were performed using a WITec CRM 200 system with excitation wavelengths of 532 and 457 nm. The laser power was kept as low as 40 μ W for all measurement to avoid heating and optical doping effects. In the doping-dependent PL measurements, 2,3,5,6-tetrafluoro-7,7,8,8-tetracyanoquinodimethane, known as a strong electron-withdrawing molecule, and deionized water were utilized as dopant molecules. F₄TCNQ was prepared in the solvent of toluene with a concentration of 0.02 μ mol/mL. The molecular adsorption was introduced by drop-casting 10 μ L of F₄TCNQ onto the WS₂ sample prepared on the \sim 1 cm² SiO₂/Si substrate, which is recorded as one doping step. The sample was then dried in ambient conditions before collecting the PL spectra. In order to systematically study the effect of the molecule on the PL spectra, successive doping was performed by repeating the same process and controlling the same amount in the droplet for each doping step. To investigate the effect of H₂O on the PL of WS₂, the small droplet (\sim 10 μ L) of deionized water was placed onto the WS₂ sample, which was then covered by a coverslip. A series of PL spectra were recorded at different times to monitor the evolution.

Device Fabrication. The source and drain electrodes were made of 5/80 nm of Ni/Au by thermal evaporation and were patterned by standard electron beam lithography, followed by the lift-off process. All electrical transport measurements were measured by a Keithley 4200 SCS parameter analyzer in a vacuum system (\sim 10⁻⁵ mbar) at room temperature.

Simulation of Charge Transfer. Monolayer WS₂ was constructed by 4 \times 4 unit cell of a 2H-WS₂ crystal from experimental data. The c axis of the periodic supercell was large enough (about 18.5 Å)

so that the interaction between the WS₂ sheet and adsorbed molecule of the adjacent supercell was negligible. The geometrical optimization was carried out by use of the GGA/PW91 method with OBS correction. The pseudopotentials are norm-conserving with a 650 eV energy cutoff. The max force is 0.02, and the max stress is 0.03 GPa. All the geometrical and energy calculations were performed in a Material Studio7.0 Castep module with the GGA/PW91-OBS method.⁵⁹

Conflict of Interest: The authors declare no competing financial interest.

Acknowledgment. This work is supported by the Singapore National Research Foundation under NRF RF award No. NRF-RF2010-07, MOE Tier 2 MOE2012-T2-2-049, and A*Star SERC PSF grant 1321202101. We thank Jiwei Li for the discussion on the charge transfer mechanism.

Supporting Information Available: The evolution of PL spectra of 1L WS₂ upon sequential doping with F₄TCNQ; variations of energies of the trion and the exciton peaks and the trion dissociation energy with the doping step; calculation of doping-dependent PL intensity of 1L WS₂ by use of the rate equations. This material is available free of charge via the Internet at <http://pubs.acs.org>.

REFERENCES AND NOTES

- Wang, Q. H.; Kalantar-Zadeh, K.; Kis, A.; Coleman, J. N.; Strano, M. S. Electronics and Optoelectronics of Two-Dimensional Transition Metal Dichalcogenides. *Nat. Nanotechnol.* **2012**, *7*, 699–712.
- Chhowalla, M.; Shin, H. S.; Eda, G.; Li, L. J.; Loh, K. P.; Zhang, H. The Chemistry of Two-Dimensional Layered Transition Metal Dichalcogenide Nanosheets. *Nat. Chem.* **2013**, *5*, 263–275.
- Jariwala, D.; Sangwan, V. K.; Lauhon, L. J.; Marks, T. J.; Hersam, M. C. Emerging Device Applications for Semiconducting

- Two-Dimensional Transition Metal Dichalcogenides. *ACS Nano* **2014**, *8*, 1102–1120.
4. Pospischil, A.; Furchi, M. M.; Mueller, T. Solar-Energy Conversion and Light Emission in an Atomic Monolayer p-n Diode. *Nat. Nanotechnol.* **2014**, *9*, 257–261.
 5. Jo, S.; Ubrig, N.; Berger, H.; Kuzmenko, A. B.; Morpurgo, A. F. Mono- and Bilayer WS₂ Light-Emitting Transistors. *Nano Lett.* **2014**, *14*, 2019–2025.
 6. Ross, J. S.; Klement, P.; Jones, A. M.; Ghimire, N. J.; Yan, J.; Mandrus, D. G.; Taniguchi, T.; Watanabe, K.; Kitamura, K.; Yao, W.; *et al.* Electrically Tunable Excitonic Light-Emitting Diodes Based on Monolayer WSe₂ p-n Junctions. *Nat. Nanotechnol.* **2014**, *9*, 268–272.
 7. Baugher, B. W. H.; Churchill, H. O. H.; Yang, Y. F.; Jarillo-Herrero, P. Optoelectronic Devices Based on Electrically Tunable p-n Diodes in a Monolayer Dichalcogenide. *Nat. Nanotechnol.* **2014**, *9*, 262–267.
 8. Lopez-Sanchez, O.; Lembke, D.; Kayci, M.; Radenovic, A.; Kis, A. Ultrasensitive Photodetectors Based on Monolayer MoS₂. *Nat. Nanotechnol.* **2013**, *8*, 497–501.
 9. Cao, T.; Wang, G.; Han, W. P.; Ye, H. Q.; Zhu, C. R.; Shi, J. R.; Niu, Q.; Tan, P. H.; Wang, E.; Liu, B. L.; *et al.* Valley-Selective Circular Dichroism of Monolayer Molybdenum Disulfide. *Nat. Commun.* **2012**, *3*, 887.
 10. Zeng, H. L.; Dai, J. F.; Yao, W.; Xiao, D.; Cui, X. D. Valley Polarization in MoS₂ Monolayers by Optical Pumping. *Nat. Nanotechnol.* **2012**, *7*, 490–493.
 11. Mak, K. F.; He, K. L.; Shan, J.; Heinz, T. F. Control of Valley Polarization in Monolayer MoS₂ by Optical Helicity. *Nat. Nanotechnol.* **2012**, *7*, 494–498.
 12. Mak, K. F.; Lee, C.; Hone, J.; Shan, J.; Heinz, T. F. Atomically Thin MoS₂: A New Direct-Gap Semiconductor. *Phys. Rev. Lett.* **2010**, *105*, 136805.
 13. Zhao, W. J.; Ghorannevis, Z.; Chu, L. Q.; Toh, M. L.; Kloc, C.; Tan, P. H.; Eda, G. Evolution of Electronic Structure in Atomically Thin Sheets of WS₂ and WSe₂. *ACS Nano* **2013**, *7*, 791–797.
 14. Peimyoo, N.; Shang, J. Z.; Cong, C. X.; Shen, X. N.; Wu, X. Y.; Yeow, E. K. L.; Yu, T. Nonblinking, Intense Two-Dimensional Light Emitter: Mono Layer WS₂ Triangles. *ACS Nano* **2013**, *7*, 10985–10994.
 15. Cheiwchanamangij, T.; Lambrecht, W. R. L. Quasiparticle Band Structure Calculation of Monolayer, Bilayer, and Bulk MoS₂. *Phys. Rev. B* **2012**, *85*, 205302.
 16. Shi, H. L.; Pan, H.; Zhang, Y. W.; Yakobson, B. I. Quasiparticle Band Structures and Optical Properties of Strained Monolayer MoS₂ and WS₂. *Phys. Rev. B* **2013**, *87*, 155304.
 17. Ramasubramaniam, A. Large Excitonic Effects in Monolayers of Molybdenum and Tungsten Dichalcogenides. *Phys. Rev. B* **2012**, *86*, 115409.
 18. Zhu, B. R.; Chen, X.; Cui, X. D. Exciton Binding Energy of Monolayer WS₂. 2014, arXiv: condense matter/1403.5108v2. arXiv.org e-Print arXiv. <http://arxiv.org/abs/1403.5108v2> (accessed Jun 8, 2014).
 19. Finkelstein, G.; Shtrikman, H.; Bar-Joseph, I. I. Optical Spectroscopy of a Two-Dimensional Electron Gas near the Metal-Insulator Transition. *Phys. Rev. Lett.* **1995**, *74*, 976–979.
 20. Huard, V. V.; Cox, R. T.; Saminadayar, K.; Arnoult, A.; Tatarenko, S. Bound States in Optical Absorption of Semiconductor Quantum Wells Containing a Two-Dimensional Electron Gas. *Phys. Rev. Lett.* **2000**, *84*, 187–190.
 21. Glasberg, S.; Finkelstein, G.; Shtrikman, H.; Bar-Joseph, I. Comparative Study of the Negatively and Positively Charged Excitons in GaAs Quantum Wells. *Phys. Rev. B* **1999**, *59*, 10425.
 22. Shields, A. J.; Osborne, J. L.; Simmons, M. Y.; Pepper, M.; Ritchie, D. A. Magneto-Optical Spectroscopy of Positively Charged Excitons in GaAs Quantum Wells. *Phys. Rev. B* **1995**, *52*, 5523.
 23. Siviniant, J.; Scalbert, D.; Kavokin, A. V.; Coquillat, D.; Lascaray, J. P. Chemical Equilibrium between Excitons, Electrons, and Negatively Charged Excitons in Semiconductor Quantum Wells. *Phys. Rev. B* **1999**, *59*, 1602.
 24. Ross, J. S.; Wu, S. F.; Yu, H. Y.; Ghimire, N. J.; Jones, A. M.; Aivazian, G.; Yan, J. Q.; Mandrus, D. G.; Xiao, D.; Yao, W.; *et al.* Electrical Control of Neutral and Charged Excitons in a Monolayer Semiconductor. *Nat. Commun.* **2013**, *4*, 1474.
 25. Jones, A. M.; Yu, H. Y.; Ghimire, N. J.; Wu, S. F.; Aivazian, G.; Ross, J. S.; Zhao, B.; Yan, J. Q.; Mandrus, D. G.; Xiao, D.; *et al.* Optical Generation of Excitonic Valley Coherence in Monolayer WSe₂. *Nat. Nanotechnol.* **2013**, *8*, 634–638.
 26. Mak, K. F.; He, K. L.; Lee, C.; Lee, G. H.; Hone, J.; Heinz, T. F.; Shan, J. Tightly Bound Trions in Monolayer MoS₂. *Nat. Mater.* **2013**, *12*, 207–211.
 27. Peimyoo, N.; Yu, T.; Shang, J. Z.; Cong, C. X.; Yang, H. P. Thickness-Dependent Azobenzene Doping in Mono- and Few-Layer Graphene. *Carbon* **2012**, *50*, 201–208.
 28. Peimyoo, N.; Li, J. W.; Shang, J. Z.; Shen, X. N.; Qiu, C. Y.; Xie, L. H.; Huang, W.; Yu, T. Photocontrolled Molecular Structural Transition and Doping in Graphene. *ACS Nano* **2012**, *6*, 8878–8886.
 29. Tongay, S.; Zhou, J.; Ataca, C.; Liu, J.; Kang, J. S.; Matthews, T. S.; You, L.; Li, J. B.; Grossman, J. C.; Wu, J. Q. Broad-Range Modulation of Light Emission in Two-Dimensional Semiconductors by Molecular Physisorption Gating. *Nano Lett.* **2013**, *13*, 2831–2836.
 30. Mouri, S.; Miyauchi, Y.; Matsuda, K. Tunable Photoluminescence of Monolayer MoS₂ via Chemical Doping. *Nano Lett.* **2013**, *13*, 5944–5948.
 31. Zeng, H. L.; Liu, G. B.; Dai, J. F.; Yan, Y. J.; Zhu, B. R.; He, R. C.; Xie, L.; Xu, S. J.; Chen, X. H.; Yao, W.; *et al.* Optical Signature of Symmetry Variations and Spin-Valley Coupling in Atomically Thin Tungsten Dichalcogenides. *Sci. Rep.* **2013**, *3*, 1608.
 32. Kuc, A.; Zibouche, N.; Heine, T. Influence of Quantum Confinement on the Electronic Structure of the Transition Metal Sulfide TS₂. *Phys. Rev. B* **2011**, *83*, 245213.
 33. Klein, A.; Tiefenbacher, S.; Eyert, V.; Pettenkofer, C.; Jaegermann, W. Electronic Band Structure of Single-Crystal and Single-Layer WS₂: Influence of Interlayer van der Waals Interactions. *Phys. Rev. B* **2001**, *64*, 205416.
 34. Zhao, W. J.; Ribeiro, R. M.; Toh, M. L.; Carvalho, A.; Kloc, C.; Neto, A. H. C.; Eda, G. Origin of Indirect Optical Transitions in Few-Layer MoS₂, WS₂, and WSe₂. *Nano Lett.* **2013**, *13*, 5627–5634.
 35. Ramasubramaniam, A.; Naveh, D.; Towe, E. Tunable Band Gaps in Bilayer Transition-Metal Dichalcogenides. *Phys. Rev. B* **2011**, *84*, 205325.
 36. Yun, W. S.; Han, S. W.; Hong, S. C.; Kim, I. G.; Lee, J. D. Thickness and Strain Effects on Electronic Structures of Transition Metal Dichalcogenides: 2H-MX₂ Semiconductors (M = Mo, W; X = S, Se, Te). *Phys. Rev. B* **2012**, *85*, 33305.
 37. Radisavljevic, B.; Radenovic, A.; Brivio, J.; Giacometti, V.; Kis, A. Single-Layer MoS₂ Transistors. *Nat. Nanotechnol.* **2011**, *6*, 147–150.
 38. Zhang, Y.; Zhang, Y. F.; Ji, Q. Q.; Ju, J.; Yuan, H. T.; Shi, J. P.; Gao, T.; Ma, D. L.; Liu, M. X.; Chen, Y. B.; *et al.* Controlled Growth of High-Quality Monolayer WS₂ Layers on Sapphire and Imaging Its Grain Boundary. *ACS Nano* **2013**, *7*, 8963–8971.
 39. Lee, Y. H.; Yu, L. L.; Wang, H.; Fang, W. J.; Ling, X.; Shi, Y. M.; Lin, C. T.; Huang, J. K.; Chang, M. T.; Chang, C. S.; *et al.* Synthesis and Transfer of Single-Layer Transition Metal Disulfides on Diverse Surfaces. *Nano Lett.* **2013**, *13*, 1852–1857.
 40. Late, D. J.; Liu, B.; Matte, H. S. S. R.; Dravid, V. P.; Rao, C. N. R. Hysteresis in Single-Layer MoS₂ Field Effect Transistors. *ACS Nano* **2012**, *6*, 5635–5641.
 41. Yin, Z. Y.; Li, H.; Li, H.; Jiang, L.; Shi, Y. M.; Sun, Y. H.; Lu, G.; Zhang, Q.; Chen, X. D.; Zhang, H. Single-Layer MoS₂ Phototransistors. *ACS Nano* **2012**, *6*, 74–80.
 42. Liu, B.; Chen, L.; Liu, G.; Abbas, A. N.; Fathi, M.; Zhou, C. High-Performance Chemical Sensing Using Schottky-Contacted Chemical Vapor Deposition Grown Monolayer MoS₂ Transistors. *ACS Nano* **2014**, *8*, 5304–5314.
 43. Mitioglu, A. A.; Plochocka, P.; Jadcak, J. N.; Escoffier, W.; Rikken, G. L. J. A.; Kulyuk, L.; Maude, D. K. Optical Manipulation of the Exciton Charge State in Single-Layer Tungsten Disulfide. *Phys. Rev. B* **2013**, *88*, 245403.
 44. Vercik, A.; Gobato, Y. G.; Brasil, M. J. S. P. Thermal Equilibrium Governing the Formation of Negatively Charged

- Excitons in Resonant Tunneling Diodes. *J. Appl. Phys.* **2002**, *92*, 1888–1892.
45. Warburton, R. J.; Schaflein, C.; Haft, D.; Bickel, F.; Lorke, A.; Karrai, K.; Garcia, J. M.; Schoenfeld, W.; Petroff, P. M. Optical Emission from a Charge-Tunable Quantum Ring. *Nature* **2000**, *405*, 926–929.
 46. Castellanos-Gomez, A.; Roldan, R.; Cappelluti, E.; Buscema, M.; Guinea, F.; van der Zant, H. S. J.; Steele, G. A. Local Strain Engineering in Atomically Thin MoS₂. *Nano Lett.* **2013**, *13*, 5361–5366.
 47. Wang, Y. L.; Cong, C. X.; Qiu, C. Y.; Yu, T. Raman Spectroscopy Study of Lattice Vibration and Crystallographic Orientation of Monolayer MoS₂ under Uniaxial Strain. *Small* **2013**, *9*, 2857–2861.
 48. Chakraborty, B.; Bera, A.; Muthu, D. V. S.; Bhowmick, S.; Waghmare, U. V.; Sood, A. K. Symmetry-Dependent Phonon Renormalization in Monolayer MoS₂ Transistor. *Phys. Rev. B* **2012**, *85*, 161403.
 49. Horzum, S.; Sahin, H.; Cahangirov, S.; Cudazzo, P.; Rubio, A.; Serin, T.; Peeters, F. M. Phonon Softening and Direct to Indirect Band Gap Crossover in Strained Single-Layer MoSe₂. *Phys. Rev. B* **2013**, *87*, 125415.
 50. Kang, J.; Tongay, S.; Zhou, J.; Li, J. B.; Wu, J. Q. Band Offsets and Heterostructures of Two-Dimensional Semiconductors. *Appl. Phys. Lett.* **2013**, *102*, 12111.
 51. Gao, W. Y.; Kahn, A. Controlled p-Doping of Zinc Phthalocyanine by Coevaporation with Tetrafluorotetracyanoquinodimethane: A Direct and Inverse Photoemission Study. *Appl. Phys. Lett.* **2001**, *79*, 4040.
 52. Sercombe, D.; Schwarz, S.; Del Pozo-Zamudio, O.; Liu, F.; Robinson, B. J.; Chekhovich, E. A.; Tartakovskii, I. I.; Kolosov, O.; Tartakovskii, A. I. Optical Investigation of the Natural Electron Doping in Thin MoS₂ Films Deposited on Dielectric Substrates. *Sci. Rep.* **2013**, *3*, 3489.
 53. Scheuschner, N.; Ochedowski, O.; Kaulitz, A. M.; Gillen, R.; Schleberger, M.; Maultzsch, J. Photoluminescence of Free-standing Single- and Few-Layer MoS₂. *Phys. Rev. B* **2014**, *89*, 125406.
 54. Dolui, K.; Rungger, I.; Sanvito, S. Origin of the n-Type and p-Type Conductivity of MoS₂ Monolayers on a SiO₂ Substrate. *Phys. Rev. B* **2013**, *87*, 165402.
 55. Zhou, W.; Zou, X. L.; Najmaei, S.; Liu, Z.; Shi, Y. M.; Kong, J.; Lou, J.; Ajayan, P. M.; Yakobson, B. I.; Idrobo, J. C. Intrinsic Structural Defects in Monolayer Molybdenum Disulfide. *Nano Lett.* **2013**, *13*, 2615–2622.
 56. Elias, A. L.; Perea-Lopez, N.; Castro-Beltran, A.; Berkdemir, A.; Lv, R. T.; Feng, S. M.; Long, A. D.; Hayashi, T.; Kim, Y. A.; Endo, M.; *et al.* Controlled Synthesis and Transfer of Large-Area WS₂ Sheets: From Single Layer to Few Layers. *ACS Nano* **2013**, *7*, 5235–5242.
 57. Sun, L. F.; Hu, H. L.; Zhan, D.; Yan, J. X.; Liu, L.; Teguh, J. S.; Yeow, E. K. L.; Lee, P. S.; Shen, Z. X. Plasma Modified MoS₂ Nanoflakes for Surface Enhanced Raman Scattering. *Small* **2014**, *10*, 1090–1095.
 58. Nan, H. Y.; Wang, Z. L.; Wang, W. H.; Liang, Z.; Lu, Y.; Chen, Q.; He, D. W.; Tan, P. H.; Miao, F.; Wang, X. R.; *et al.* Strong Photoluminescence Enhancement of MoS₂ through Defect Engineering and Oxygen Bonding. *ACS Nano* **2014**, *8*, 5738–5745.
 59. Ortmann, F.; Bechstedt, F.; Schmidt, W. G. Semiempirical van der Waals Correction to the Density Functional Description of Solids and Molecular Structures. *Phys. Rev. B* **2006**, *73*, 205101.